https://doi.org/10.2352/ISSN.2470-1173.2021.15.COIMG-229

Enhanced Material Estimation with Multi-Spectral CT

Sandamali Devadithya, David Castañón; Boston University; Boston, MA/U.S.A.

Abstract

Conventional X-ray computed tomography (CT) systems obtain single- or dual-energy measurements, from which dual-energy CT has emerged as the superior way to recognize materials. Recently photon counting detectors have facilitated multi-spectral CT which captures spectral information by counting photon arrivals at different energy windows. However, the narrow energy bins result in a lower signal-to-noise ratio in each bin, particularly in the lower energy bins. This effect is significant and challenging when high-attenuation materials such as metal are present in the area to be imaged. In this paper, we propose a novel technique to estimate material properties with multi-spectral CT in the presence of high-attenuation materials. Our approach combines basis decomposition concepts using multiple-spectral bin information, as well as individual energy bin reconstructions. We show that this approach is robust in the presence of metal and outperforms alternative techniques for material estimation with multi-spectral CT as well with the state-of-art dual-energy CT.

Introduction

Non-destructive material characterization is important in many applications related to medical, security, and industrial imaging. X-ray computed tomography (CT) offers the potential of estimating material properties such as effective atomic number and density which helps to characterize the materials present. In order to estimate such properties, dual-energy CT (DECT) is utilized, where objects are scanned with two distinct X-ray energy spectra. However, the reconstructed images from the measurements of each individual spectrum contain significant artifacts due to monochromatic approximations used in the inversion algorithms, and to the low signal levels caused by the presence of highly-attenuating materials. The linear attenuation coefficient (LAC), which characterises the attenuation of the X-ray beam as it travels through the object, is energy-dependent. In CT systems, the reconstruction algorithms often assume a monochromatic X-ray beam model, which results in beam hardening [1] and other artifacts leading to poor material characterization.

To alleviate beam hardening artifacts in dual-energy systems, images are often generated as coefficients of energy-dependent basis functions. The detector measurements in the two energy spectra are decomposed into basis coefficient measurements, from which coefficient images are subsequently reconstructed [2, 3]. These basis images then can be used to estimate material properties such as effective atomic number and electron density.

However, the presence of metal or other dense materials which have a higher absorption rate leads to significant distortions in the reconstructed basis images, because the lower energy photons are heavily attenuated. These distortions can lead to inaccurate material characterization in security imaging. In our prior work [4] we proposed a reconstruction technique based on minimizing weighted least squares estimation with edge-preserving total variation regularization for the most common basis functions of photoelectric absorption and Compton scatter basis (PCB) functions. While the proposed method outperformed the competing iterative reconstruction algorithms, the final photoelectric images still had some artifacts. The photoelectric absorption rate at lower energies is significantly higher in metal, and is difficult to estimate given the detector measurements. Therefore in [5] we investigated alternative basis functions of synthesized monochromatic basis (SMB) [6] which performed significantly better than PCB functions in the presence of metal.

In this paper we utilize multi spectral CT (also known as multi-energy CT (MECT)) for material estimation in the presence of metal. Different from DECT, MECT systems count photon arrivals at narrow energy windows with photon counting detectors, allowing for the formation of CT images in each energy window. In this manner, MECT systems capture more spectral dependent information [7]. Since the energy bins are narrow, there will be little beam hardening artifacts as compared with conventional CT, and the attenuation values in CT images can be directly interpreted as estimates of the LAC values at different energies. In [8], a method was proposed to estimate effective atomic number and electron density directly from the energy dependent CT images. A limitation of this approach is that the number of photons measured in each energy bin is much less than that with conventional energy-integrating detectors, and results in a lower signal to noise ratio (SNR). This becomes a significant issue in the presence of dense materials particularly as the lower energy bins have only a few photons to use for the reconstructions.

We propose to estimate material properties by combining direct energy bin reconstructions and basis image reconstructions. In [9] and [10] basis decomposition reconstruction was achieved with multi-spectral CT measurements. In [9] a DECT sinogram decomposition method of using PCB functions was extended for MECT and basis images were reconstructed with FBP. In [10] a new basis representation was introduced to represent K-edge materials. However none of these work addressed material characterization of scenes containing significant metal regions.

In this paper we propose a robust novel technique to estimate material properties in the presence of metal, exploiting MECT measurements. Building on our prior work on DECT [4], we use down-weighted sinograms and edge-preserving total variation (EPTV) regularization for image reconstruction. We first estimate the basis sinograms from the measurements in all energy bins using a weighted non linear solver. The weighting serves to de-emphasize energy bins which have low photon counts. Next, we do an initial reconstruction of the highest energy image to determine edges for regions in the reconstructed image, in order to support EPTV reconstruction of the basis images. This energy

bin has the strongest SNR, which enables accurate determination of region boundaries. We also use EPTV regularization to get an enhanced image of the highest-energy bin. Once we have the three images (dual basis images and the high energy direct image), we estimate the effective atomic number and the electron density.

We compare the proposed method with alternative techniques for material estimation with MECT and state-of-art DECT in the presence of metal. We used DECT experimental results acquired from a Imatron C300 medical scanner to determine representative containers with multiple materials present. We add materials of interest and metal to those containers and simulate both DECT and MECT signatures. We used two different basis decompositions, one based on a pair of materials (aluminum and polystyrene), and a second based on synthesized monochromatic basis (SMB). Our experiments indicate that our proposed method generates more accurate estimates of effective atomic number and electron density over a broad range of conditions.

In the following sections we give an overview of MECT modality, a detailed description of the proposed algorithm and describe our performance evaluation experiments.

Measurement Model

Multi-spectral CT systems count photon arrivals in narrow energy windows with Photon Counting Detectors (PCD). The Beer-Lambert law indicates that the expected photon counts received at detector j can be modelled as

$$I_i(j) = \int I_0 w_i(E) e^{-\int_{L_j} \mu(r,E)dl} dE \tag{1}$$

with $i = 1...N$ denoting the energy bins and $w_i(E)$ denoting the narrow spectrum at the energy bin i which includes the energy-dependent source strength and detector sensitivity. In this equation, E is the energy level, r is the spatial location, $\mu(r,E)$ is the linear attenuation coefficient (LAC) at energy E and position r along the X-ray path L_j, and I_0 is the source intensity. In Figure 1 we show an example multi-energy spectra with 9 bins.

Note that the actual received counts at detector j are modeled as a Poisson process with the mean given by (1), neglecting electronic noise in this approximation. We use the negative log of the normalized intensity of photon counts as the measurements quantities in each energy bin, which are referred to as sinograms when collected over all detectors. Let $s_i(j)$ denote the measured i^{th} energy sinogram at detector j, defined as

$$s_i(j) = -\ln\left(\frac{Z_i(j)}{Z_{i,0}(j)}\right) \tag{2}$$

where $Z_i(j)$ are the actual received counts and $Z_{i,0}(j)$ are the expected photon counts from a direct path with no attenuation on projection L_j.

Dual-energy CT systems collect only two measurements of the scene acquired with two distinct X-ray spectral distributions, each of which is significantly wider in support over photon energies. An advantage of using narrow energy bins in MECT is the capture of additional spectrally-dependent information, as well as the relative homogeneity of photon energies in each energy bin. This latter effect can alleviate beam hardening that arises with wider spectra. In particular, one can form CT images in each energy window and estimate the LAC values directly at each center energy. However, the narrow energy bins reduces the number of photons measured in each energy bin, which leads to lower signal to noise ratio (SNR). In the presence of metal this becomes a significant issue, particularly in the lower energy bins where photons are heavily attenuated. In order to avoid this, one can use basis decomposition techniques using the multispectral measurements, enabling combination of multiple energy windows to estimate basis coefficients accurately. These basis coefficients can be used to reconstruct the basis images, and estimate material properties from them.

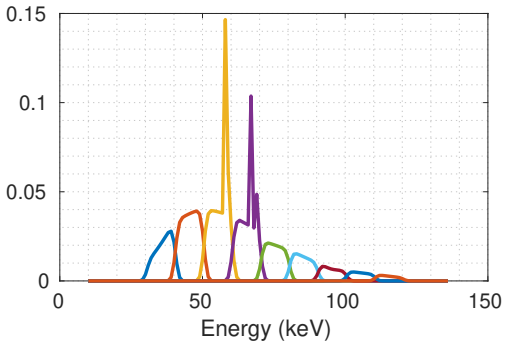

Figure 1: An example of multi-energy spectra with 9 bins

In dual basis decomposition, the energy-dependent LAC of a material is approximated in terms of two energy-dependent basis functions $f_1(E)$ and $f_2(E)$ as

$$\mu(r,E) = x_1(r) f_1(E) + x_2(r) f_2(E) \tag{3}$$

where $x_1(r)$ and $x_2(r)$ are the respective basis coefficients of the material at spatial location r. Using this basis decomposition, the expected value of normalized counts in (1) can be written as

$$I_i(j) = \int w_i(E) e^{-\int_{L_j} (x_1(r) f_1(E) + x_2(r) f_2(E))dl} dE \tag{4}$$

which can be further simplified as

$$I_i(j) = \int w_i(E) e^{-y_1(j) f_1(E) - y_2(j) f_2(E)} dE \tag{5}$$

where $y_1(j) = \int_{L_j} x_1(r)dl$ and $y_2(j) = \int_{L_j} x_2(r)dl$ are line integrals of basis coefficients along the ray L_j.

The first step in multi-energy basis image reconstruction is to decompose the energy bin measurements at detector j, denoted by $s_1(j)...s_N(j)$ into the basis integrals $y_1(j), y_2(j)$. We do this using a nonlinear least squares minimization, where we minimize

$$\min_{y_1,y_2} \sum_{i=1}^{N} Z_i(j)(s_i(j) + \ln \int w_i(E) e^{-y_1 f_1(E) - y_2 f_2(E)} dE)^2 \tag{6}$$

Here we use the measured counts as an approximation to the inverse variance of the measurements, as in [11]. This weighting de-emphasizes energy bins which have low photon counts. We use a trust-region algorithm to solve the non linear problem, with Steihaug's conjugate gradient method used to solve the trust-region sub-problem [12]. We vectorize the problem such that a GPU can be utilized for the estimation to obtain the decomposition for all detectors j in parallel.

We refer to the collection of decomposed measurements $y_1(j), y_2(j)$ for the different detectors as basis sinograms. Discretizing the relationship of the basis sinograms with the respective basis coefficients using the forward projection matrix $\mathbf{A}$, we obtain the linear relationship

$$\mathbf{y}_1 = \mathbf{A}\mathbf{x_1} \quad \text{and} \quad \mathbf{y}_2 = \mathbf{A}\mathbf{x_2} \tag{7}$$

Once coefficient images are reconstructed, they can be used to estimate effective atomic number Z_e and electron density ρ_e. However, estimating accurate coefficient images in the presence of metal is still challenging and we describe our approach next.

Enhanced Reconstruction

In our prior work [4] we developed a regularization technique based on edge-preserving total variation (EPTV) for DECT dual-basis images utilizing the structure similarity between the basis images, where region edges were expected in similar locations in both images. In this work we extend the technique to MECT, exploiting the idea that individual images reconstructed at each energy bin and the basis images will share the same region structure. In [4], we did an initial reconstruction of the high energy image to find the edges. Here we use the highest energy bin for the initial reconstruction as it suffers less from photon starvation and has the highest SNR. Once the edges are identified, the optimization problem for generating a basis coefficient image for basis b can be modelled as,

$$\hat{\mathbf{x}}_b = \underset{\mathbf{x}_b}{\operatorname{argmin}} \frac{1}{2}||\mathbf{y}_b - \mathbf{A}\mathbf{x}_b||^2_{\mathbf{W}_b} + \tau||\mathbf{W}_h\mathbf{D}_h\mathbf{x}_b||_1 + \tau||\mathbf{W}_v\mathbf{D}_v\mathbf{x}_b||_1 \tag{8}$$

In this optimization, $\mathbf{W}_b$ is the weighting matrix used to weight the importance of different components of the basis sinogram. In solving the nonlinear least squares problem in (6), we obtain an estimate of the covariance for the basis coefficients at each detector, and we use the inverse of these covariances as the components of the diagonal matrix $\mathbf{W}_b$. $\mathbf{W}_h$ and $\mathbf{W}_v$ are diagonal matrices for edge preserving with elements assigned as $w_h = exp(\frac{-\mathbf{D}_h\mu_{high}}{\beta})$ and $w_v = exp(\frac{-\mathbf{D}_v\mu_{high}}{\beta})$, where μ_{high} is the high-energy image, $\mathbf{D}_h$ and $\mathbf{D}_v$ are horizontal and vertical gradient operators, and β is the controlling parameter. τ is the regularization parameter. We use split-Bregman techniques [13] to solve (8) and the details of the implementation steps can be found in [4].

We experimented with two sets of basis functions: material basis functions and synthesized monochromatic basis (SMB) functions. We did not use the common photoelectric and Compton basis functions, because the photoelectric basis function reconstruction is very noisy in the presence of metal, when compared to other basis functions. In material basis decomposition, the LAC values of a material is approximated by as a linear combination of the LAC values of aluminum and polystyrene. The SMB functions approximate monochromatic functions at chosen energies, so that the basis coefficients coincide with the LAC values at those energies. We chose SMB 27 and SMB 93 as our SMB functions. The basis functions are illustrated in Figure 2. The reason for choosing 27 keV and 93 keV for SMB functions, is that these energies are the most separated energies covered by both the spectra of the DECT scanner we used in our experiments.

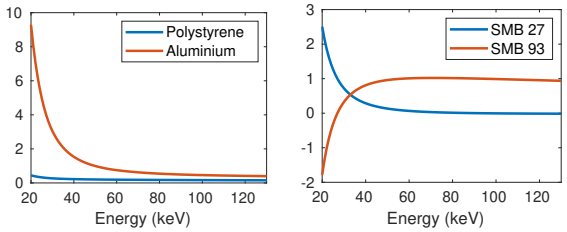

(a) (b)

Figure 2: Basis functions: (a) Material basis, (b) Synthesized monochromatic basis.

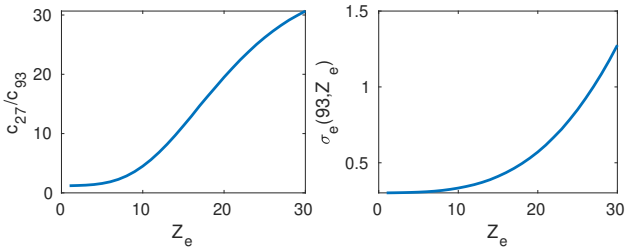

(a) (b)

Figure 3: Material estimation with LAC values, (a) ratio of LAC at 27 keV to LAC at 93 keV vs atomic number, (b) electronic attenuation at 93 keV vs atomic number.

Enhanced Material Estimation

Once the basis coefficient images are reconstructed, the linear attenuation at any two energies can be extrapolated from the basis coefficients. If using SMB functions the basis coefficients will be the LAC values at the selected energies. These two LAC values (or SMB coefficients) are used to estimate effective atomic number (Z_e) and electron density (ρ_e) as derived in detail in [6]. Suppose c_L and c_H are the estimated LAC coefficients at energies E_L and E_H. In this case, Z_e is a function of the ratio of $(\frac{c_L}{c_H})$. Once Z_e is found ρ_e can be determined by,

$$\rho_e = \frac{c_H}{\sigma_e(E_H, Z_e)} \tag{9}$$

Here $\sigma_e(E_H, Z_e)$ is the electronic attenuation at energy E_H. The relationships between Z_e and the ratio $(\frac{c_L}{c_H})$, and between Z_e and $\sigma_e(E_H, Z_e)$ for pure elements of atomic number ranging from 1 to 30 are depicted in Figure 3. We use linear interpolation to estimate Z_e and ρ_e using these curves. This is the approach we used with DECT in [5].

This approach can be enhanced utilizing the additional spectral information received with MECT. While the measurements in lower energy bins may be corrupted due to low photon counts, the measurements in higher energy bins are much cleaner. Therefore to estimate ρ_e we can directly use the attenuation at a higher energy bin. Since the bins are narrow, at higher energies the LAC curves of the materials are relatively flat with energy. Thus, we assume that the attenuation reconstructed at each energy bin is equivalent to the attenuation at the center energy of the bin.

In this work we use the highest energy bin to find ρ_e. We used an initial reconstruction of the highest energy image to find the edges for basis image reconstruction with EPTV regularization. Using the same EPTV regularization we can get an enhanced image of the highest-energy bin as

$$\hat{\mu}_H = \underset{\mu_H \geq 0}{\operatorname{argmin}} \frac{1}{2}||\mathbf{S}_H - \mathbf{A}\mu_H||^2_{\mathbf{W}_H} + \tau||\mathbf{W}_h\mathbf{D}_h\mu_H||_1 + \tau||\mathbf{W}_v\mathbf{D}_v\mu_H||_1 \tag{10}$$

Here $\mathbf{S}_H$ is the sinogram of the highest energy bin and $\mathbf{W}_H = diag(\mathbf{Z}_{high})$ where $\mathbf{Z}_{high}$ are the photon counts received at the highest energy bin.

Experiments and Results

As we do not have experimental data with MECT, we use DECT experimental results (acquired from Imatron C300 medical scanner) to determine the contents of cluttered images with various articles. We added materials of interest and additional metal structures to the regions of interest, and we simulate both DECT and MECT measurements for regions containing the background clutter, as well as added metal and materials of interest. Figure 4 shows the reconstructed SMB images of a slice from a bag with clutter acquired with the DECT scanner. We then inject a box, a bottle and various metal pieces as shown in Figure 5. The metal is positioned as in metal clutter observed in other experimental data.

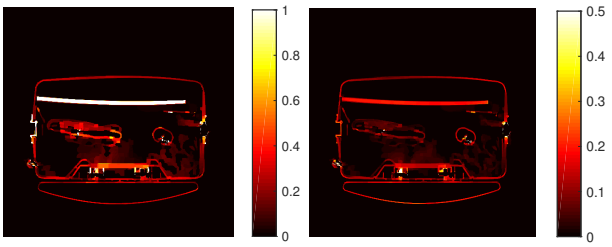

(a) (b)

Figure 4: Reconstructed SMB images from DECT scanner data (a) SMB 27, (b) SMB 93.

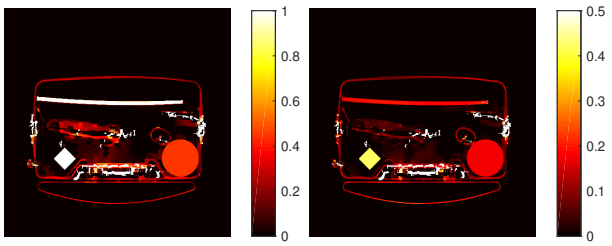

(a) (b)

Figure 5: Injected objects on the scanner data (a) SMB 27, (b) SMB 93. The bottle is filled with water and the box is filled with black powder.

We experimented with different liquids inside the bottle, and different powder materials in the box. The choice of liquids and powders were spread across the feature space of Z_e and ρ_e. For liquids, we chose water, acetone, cytric acid, ethanol, hydrochloric acid, and kerosene. For powders, we chose PETN, polypropylene (PP), RDX, calcium chloride, magnesium, and black powder. The Z_e and ρ_e of all the materials are depicted in Figure 6. The metallic pieces we added were made of copper. The material attenuation coefficients for these materials were obtained from the NIST XCOM database [14] for use in our simulations. Poisson noise was added to all detector measurements. We forward projected the attenuation values to generate both MECT and DECT data. We designed the MECT spectra illustrated in Figure 1 to match closely as possible to Imatron C300 DECT spectra (95 kVp and 130 kVp) such that the photons received at each energy were comparable for both systems. We estimate Z_e and ρ_e with our proposed MECT method, and compare them with two alternative methods: estimation with DECT basis decomposition, and estimation with MECT direct energy bin reconstructions. The process on estimating Z_e and ρ_e with DECT are laid out in detail in [5]. For estimating Z_e and ρ_e directly from MECT energy bin reconstructions, we follow the method proposed in [8]. Note that instead of finding low- and high-energy thresholds as in [8], we use all energy bins to estimate the material properties, because choosing the correct thresholds was not practical for scenes with multiple materials and lots of metal scatter. For all reconstructions, we used the EPTV regularization technique described earlier.

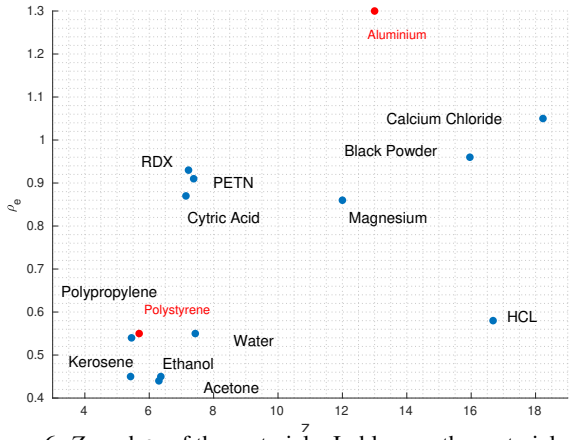

Figure 6: Z_e and ρ_e of the materials. In blue are the materials we chose to evaluate and in red are the basis materials.

The SMB reconstructions for a slice when the bottle is filled with water and the box is filled with black powder are shown in Figure 7 (the ground truth is the Figure 5). Looking closely at the figures we see that the MECT reconstructions are much sharper and cleaner than the DECT reconstructions.

Table 1: Average of relative mean errors for Z_e

Mean error (%)	DECT		MECT direct	MECT	
	MB	SMB		MB	SMB
Metal free	1.06	0.42	1.50	1.06	0.37
With metal	8.68	7.49	3.33	2.99	2.8

In tables 1 and 2 we list the relative mean absolute errors of Z_e and ρ_e. When metal is not present errors are 1% or less for both DECT and MECT basis decomposition. MECT direct estimates

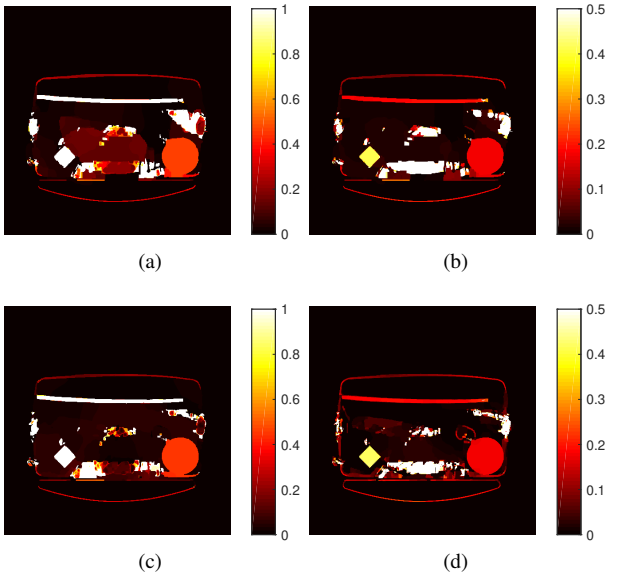

Figure 7: SMB reconstructions of the slice containing a water bottle and a black powder box; (a) DECT SMB 27, (b) DECT SMB 93, (c) MECT SMB 27, (d) MECT SMB 93.

Table 2: Average of relative mean errors for ρ_e

Mean error (%)	DECT		MECT direct	MECT		MECT-joint	
	MB	SMB		MB	SMB	MB	SMB
Metal free	0.79	0.21	1.54	0.75	0.16	0.16	0.32
With metal	10.1	2.51	2.71	4.52	1.8	0.95	1.52

have higher errors around 1.5%. This is because, even without the presence of metal, the higher Z_e materials suffer from the low photon counts in lower energy bins.

In the presence of metal, MECT estimates are clearly better than DECT estimates for both Z_e and ρ_e. To shed additional insight on these results, we show the errors for individual materials in tables 3 and 4. The average Z_e errors with DECT are $\sim 8\%$, and the average errors with MECT are $\sim 3\%$, which is a significant improvement. In addition the Z_e estimates with MECT basis decomposition are better than with the direct method.

The ρ_e errors with DECT and MECT basis decomposition again show that MECT is significantly better no matter which basis set is used, with an improvement from 10% to 5% for MB and an improvement from 2.5% to 1.8% for SMB. For the MECT direct method, the ρ_e estimates are good for low Z_e materials, but they show significant errors for high Z_e materials. ρ_e estimates with MECT MB decomposition are less accurate, when compared to the MECT estimates with SMB decomposition. This is likely due to the choice of the materials in MB. Aluminium and polystyrene are not as good as SMB at resolving the higher energy components of denser materials, and ρ_e depends mostly on the higher energy components. This can be improved by estimating ρ_e with the joint method. In the joint method instead of using the basis coefficients to estimate the high energy attenuation, we use the direct energy bin reconstruction for the high energy bin. This reduces the ρ_e errors with MB to 1%. There is also improvement

Table 3: Z_e relative mean errors of all materials in the presence of metal

Mean error (%)	DECT		MECT direct	MECT	
	MB	SMB		MB	SMB
Kerosene	25.9	7.25	4.37	10	3.03
Acetone	7.44	6.85	4.07	2.62	2.18
Ethanol	6.47	6.94	2.40	2.83	1.14
Cytric A	1.11	2.53	1.32	1.96	1.23
Water	1.98	2.62	3.34	1.52	0.34
Hcl	0.36	0.34	5.65	0.39	0.69
PP	10.9	28.5	0.41	5.02	10.5
RDX	32.4	4.32	0.47	1.99	0.32
PETN	1.94	18.7	0.22	1.38	0.59
Mg	3.55	0.85	3.71	0.48	0.41
Black P	4.21	5.04	2.44	3.36	7.87
$CaCl_2$	7.77	5.94	11.56	4.34	5.33
Average	8.68	7.49	3.33	2.99	2.8

Table 4: ρ_e relative mean errors of all materials in the presence of metal

Mean error (%)	DECT		MECT direct	MECT		MECT-joint	
	MB	SMB		MB	SMB	MB	SMB
Kerosene	4.49	1.83	0.31	2.58	0.64	1.27	1.05
Acetone	5.02	1.13	0.37	2.34	0.72	1.28	1.25
Ethanol	1.79	1.32	0.40	1.91	0.91	1.34	1.25
Cytric A	1.99	0.76	0.42	1.18	0.41	0.21	0.31
Water	3.28	0.75	0.72	2.01	0.63	1.12	1.07
Hcl	2.1	0.81	11.38	1.4	0.3	0.57	0.51
PP	2.89	7.75	0.10	2.36	0.63	0.41	0.65
RDX	8.21	3.13	0.05	4.82	0.7	0.33	0.24
PETN	18.9	1.54	0.08	5.38	0.34	0.5	0.44
Mg	16.3	3.73	2.27	0.35	1.5	0.4	0.38
Black-P	23.6	2.9	2.85	13.5	8.48	1.13	5.65
$CaCl_2$	32.7	4.43	13.58	16.3	6.35	2.89	5.47
Average	10.1	2.51	2.71	4.52	1.8	0.95	1.52

in using the joint method with SMB, particularly for higher Z_e materials, but the overall improvement is not as dramatic, as the SMB 93 basis is capable of capturing the higher energies components well. The joint method is much useful when the basis functions cannot extrapolate high energy components accurately.

Discussion

In this paper we presented a robust algorithm to estimate material properties in the presence of metal, utilizing multi-spectral CT (MECT). We extended edge-preserving total variation regularization for enhanced image reconstruction and combined basis image reconstructions and direct energy bin reconstructions to estimate Z_e and ρ_e. The proposed method outperformed the alternative techniques of estimating materials from direct MECT reconstructions and the state-of-art DECT techniques. The main limitation of the proposed approach is that it is more computationally complex than standard back-projection algorithms but the computations can be structured to exploit parallelism.

We experimented with two choices of basis functions: material bases (MB) and synthesized monochromatic bases (SMB). When analysing the results on accuracy of estimation for Z_e and ρ_e, MB and SMB behaved differently for different materials. There is still ambiguity as to the optimal choice of basis functions and the energies for material recognition. This is a topic for further investigation.

References

[1] A. C. Kak, M. Slaney, and G. Wang, "Principles of computerized tomographic imaging," Medical Physics, vol. 29, no. 1, pp. 107–107, 2002.

[2] S. G. Azevedo, H. E. Martz, M. B. Aufderheide, W. D. Brown, K. M.Champley, J. S. Kallman, G. P. Roberson, D. Schneberk, I. M. Seetho, and J. A. Smith, "System-independent characterization of materials using dual-energy computed tomography," IEEE Transactions on Nuclear Science, vol. 63, no. 1, pp. 341–350, 2016.

[3] R. E. Alvarez and A. Macovski, "Energy-selective reconstructions in X-ray computerised tomography," Physics in Medicine & Biology, vol. 21, no. 5, p. 733, 1976.

[4] S. Devadithya and D. Castañón, "Edge-preserving total variation regularization for dual-energy CT images," Electronic Imaging, vol. 2019, no. 13, pp. 147–154, 2019.

[5] S. Devadithya and D. Castañón, "Material identification in presence of metal for baggage screening," Electronic Imaging, vol. 2020, no. 14, 2020.

[6] K. M. Champley, S. G. Azevedo, I. M. Seetho, S. M. Glenn, L. D.McMichael, J. A. Smith, J. S. Kallman, W. D. Brown, and H. E. Martz, "Method to extract system-independent material properties from dual-energy X-ray CT," IEEE Transactions on Nuclear Science, vol. 66, no. 3, pp. 674–686, 2019.

[7] X. Wang, D. Meier, K. Taguchi, D. J. Wagenaar, B. E. Patt, and E. C. Frey, " Material separation in X-ray CT with energy resolved photon-counting detectors," Medical physics,vol. 38, no. 3, pp. 1534-1546, 2011.

[8] M. Busi, K. A. Mohan, A. A. Dooraghi, K. M. Champley, H. E. Martz, and U. L. Olsen, "Method for system-independent material characterization from spectral X-ray CT," NDT & E International, vol. 107, p. 102136, 2019.

[9] Y. Yaoshen, B.Tracey, and E. Miller. "Robust X-ray based material identification using multi-energy sinogram decomposition." Anomaly Detection and Imaging with X-Rays (ADIX). Vol. 9847. International Society for Optics and Photonics, 2016.

[10] P. Babaheidarian and D. Castañón, "Feature selection for material identification in spectral CT," Electronic Imaging, vol. 2018, no. 15, 2018.

[11] K. Sauer, and C.Bouman, "A local update strategy for iterative reconstruction from projections", IEEE Transactions on Signal Processing, V.41, No.2 (1993).

[12] T. Steihaug, "The conjugate gradient method and trust regions in larges cale optimization," SIAM Journal on Numerical Analysis, vol. 20, no. 3, pp. 626–637, 1983.

[13] T. Goldstein and S. Osher, "The split Bregman method for L1-regularized problems," SIAM journal on imaging sciences, vol. 2, no. 2, pp. 323–343, 2009.

[14] M. J. Berger and J. Hubbell, "Xcom: Photon cross sections on a personal computer," tech. rep., National Bureau of Standards, Washington, DC(USA). Center for Radiation, 1987.

Author Biography

Sandamali Devadithya received the B.Sc. in electronics and telecommunication engineering from the University of Moratuwa, Sri Lanka (2013), and the M.S.E.E. from the University of Washington, Seattle, USA (2017). She is currently a Ph.D. candidate at the Department of Electrical and Computer Engineering, Boston University, Boston, USA. Her current research interests include computational imaging and sensing, inverse problems, and digital signal processing.

David Castañón is Professor of Electrical and Computer Engineering at Boston University. He received his Ph.D. in applied mathematics from MIT (1976). He was Chief Scientist at ALPHATECH before joining Boston University (1990). He has been ECE Department Chair, co-director of the Center for Information and Systems Engineering, President of the IEEE Control Systems Society, and member of Air Force's Scientific Advisory Board. His interests include control, estimation, optimization, inverse problems and image understanding.

JOIN US AT THE NEXT EI!

IS&T International Symposium on

Electronic Imaging

SCIENCE AND TECHNOLOGY

Imaging across applications . . . Where industry and academia meet!

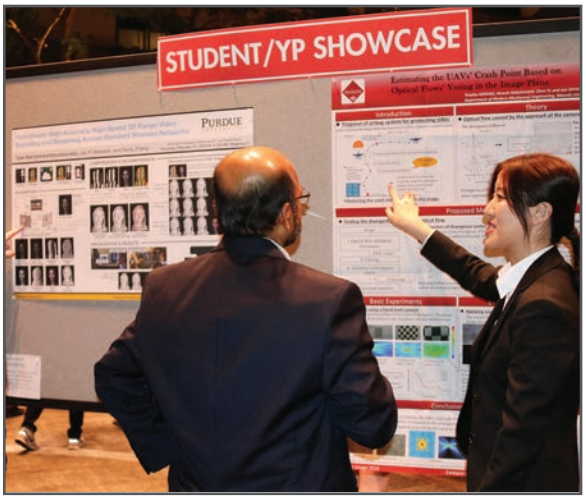

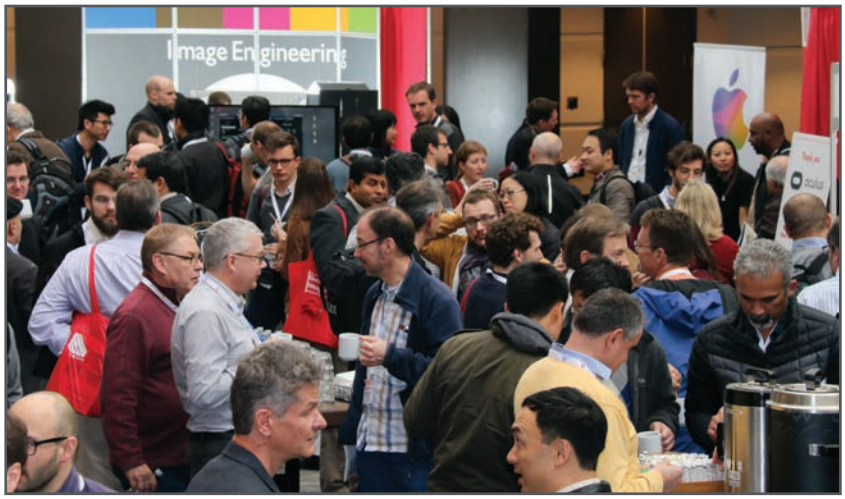

• SHORT COURSES • EXHIBITS • DEMONSTRATION SESSION • PLENARY TALKS •
• INTERACTIVE PAPER SESSION • SPECIAL EVENTS • TECHNICAL SESSIONS •

www.electronicimaging.org

IS&T
imaging.org